

Received July 13, 2018, accepted August 16, 2018, date of publication August 28, 2018, date of current version September 21, 2018.

Digital Object Identifier 10.1109/ACCESS.2018.2867494

Multiwindow Nonharmonic Analysis Method for Gravitational Waves

**DONGBAO JIA^{1,2}, KENTA YANAGISAWA², YUTA ONO², KANNA HIROBAYASHI²,
MASAYA HASEGAWA², SHIGEKI HIROBAYASHI², (Member, IEEE), HIDEYUKI TAGOSHI³,
TATSUYA NARIKAWA^{3,4}, NAMI UCHIKATA^{3,5}, AND HIROTAKA TAKAHASHI⁶**

¹School of Computer Engineering, Huaihai Institute of Technology, Lianyungang 222005, China

²Graduate School of Science and Engineering, University of Toyama, Toyama 930-8555, Japan

³Institute for Cosmic Ray Research, The University of Tokyo, Kashiwa 277-8582, Japan

⁴Department of Physics, Kyoto University, Kyoto 606-8502, Japan

⁵Graduate School of Science and Technology, Niigata University, Niigata 950-2181, Japan

⁶Department of Information and Management Systems Engineering, Nagaoka University of Technology, Nagaoka 940-2188, Japan

Corresponding author: Shigeki Hirobayashi (hirobays@eng.u-toyama.ac.jp)

This work was supported by the JSPS KAKENHI under Grant 15H00779 and Grant 18H03259.

ABSTRACT The frequency of the observed gravitational wave (GW) signal GW150914 changes slowly over a long time in the low frequency band and then increases rapidly from low to high frequency band, the frequency variance over time of such signals cannot be analyzed and visualized accurately using current analytical methods due to their fixed analytical window lengths or low time-frequency resolutions. To obtain high-accuracy GW representations, we propose the use of multiwindow nonharmonic analysis (NHA); in this method, NHA is performed using different window lengths for each subband after a band division procedure. A simulated signal was used to compare the results obtained using NHA and multiwindow NHA in this paper. The results distinctly show that the error of multiwindow NHA is 6.311 Hz which is lower than NHA. We also compared the results of multiwindow NHA with those of state-of-the-art methods by using actual GW150914 data and verified the analytical precision of these techniques. We found that the high time-frequency resolution of multiwindow NHA and its low sensitivity to analysis window variations enable it to analyze more accurately with 6.021 Hz errors in the extracted interval than the state-of-the-art methods even with the presence of significant noise. In addition, only multiwindow NHA can accurately represent GW signals at amplitudes down to the noise limit and achieve correct low-frequency range representation, due to its ability to assign the appropriate window length for each subband.

INDEX TERMS Gravitational wave, band division, analytical window length, nonharmonic analysis (NHA), multiwindow NHA.

I. INTRODUCTION

The existence of gravitational waves (GWs), first predicted based on Einstein's theory of relativity, has been proven only indirectly [1]. GWs were first detected by the Laser Interferometer Gravitational-Wave Observatory (LIGO) detectors in Hanford, Washington state, and Livingston, Louisiana, USA on September 14, 2015; this event was named GW150914 [2]–[4]. This observation was heralded as inaugurating a new era of gravitational-wave astronomy, that will enable observations of violent astrophysical events that were not previously possible, and potentially allow direct observation of the very earliest history of the universe [2], [3]. Laser-interferometer-based GW detectors currently in operation include LIGO [5], [6], the Virgo interferometer [7], [8], and the Kamioka Gravitational Wave Detector (KAGRA) [9], [10].

GW signals can originate from several different sources, such as coalescence of two neutron stars, coalescence of a neutron star and a black hole, and coalescence of two black holes [11], [12]; the latter cosmic event is thought to have generated the observed GW150914 signal [2]. In addition to the GW150914 event, several GW events have been detected, such as GW151226 [13], GW170104 [14], GW170608 [15], GW170814 [16], and GW170817 [17]. The time of GW occurrence can only be detected using a matched filter [18], [19], but it is difficult to extract frequency changes accurately along the timeline of a GW event. Therefore, GW analysis must be performed using time-frequency analysis [20].

Moreover, in the actual analysis, the measurement data acquired by such detectors are influenced by the various noises caused by power supply noise, photon shot noise,

etc., which are significantly larger than the typical GW observation signals [2], [21], [22]. These noises seriously affect the observation and analysis of GW signal in time-frequency domain. Therefore, the time-frequency analysis method needs a high frequency resolution and noise rejection capability.

For GW time-frequency analysis, there are several time-frequency analysis methods. For example, short-time Fourier transforms (STFTs) [23]–[25] are commonly used to confirm the frequency of sine wave in a local area of a time-varying signal. Wavelet transforms [2], [13]–[17], [26], [27] are the most widely used for the time-frequency analysis of GW signal at present. Furthermore, in 2017, a new multicomponent signal analysis method for GW signals called the Fourier-based synchrosqueezing transform (FSST) method was proposed [28]. Although each of these methods has its own characteristics and advantages, as the influence of noise and the frequency of GW signal changes differently at the different period, it is difficult to analyze and extract the frequency changes of a GW signal accurately.

In this paper, we propose a new method called multiwindow nonharmonic analysis (NHA) to improve the analytical precision of GW signal in time-frequency domain by using the simulated and actual signals. According to the analysis of the simulated signal, the proposed method is clarified to be progressive and feasible for the GW analysis; and by analyzing the actual signal, we experimentally demonstrate the proposed method can effectively improve the time-frequency resolution and noise rejection capability than the state-of-the-art methods.

II. RELATED WORKS

STFT is the most widely used method in time-frequency analysis; if the period of a signal is constant, highly accurate analysis results can be obtained. However, for signals with variable frequencies, such as GWs, as the analytical window length can significantly influence the analytical precision of STFT [29], it is difficult to analyze signals whose periods are not constants; therefore, the analytical precision decreases. Furthermore, as the analytical window length needs to be fixed according to the frequency, it is difficult to achieve the compatibility between the time and frequency resolutions. Hence, if the window length is short, the frequency resolution decreases, whereas the time resolution decreases in the case of a long window length. Therefore, STFT is unsuitable for GW analysis.

Wavelet transforms are useful for analyzing time series with different time scales or changes in variance, and wavelet analysis is used to determine the dominant modes of a signal and its evolution with time. It also enables easier detection of short-duration events within large series of time [30]. Furthermore, the basis function is scaled, making it possible to analyze a wide frequency domain; however, wavelet transforms yield poor time resolution in the low-frequency range and poor frequency resolution in the high-frequency

range [31], [32]. Consequently, it is difficult to represent the frequency variation of a signal accurately.

FSST as a new multicomponent signal analysis method was proposed in 2017. This technique provides a highly concentrated time-frequency representation for a wide variety of AM-FM multicomponent signals and enables reconstruction of their modes with high accuracy. However, the FSST technique is still based on the STFT method, which is strongly influenced by the analytical window length and preprocessing method variability. Therefore, questions regarding its improvement relative to the STFT method and sensitivity to preprocessing changes make its effectiveness unclear.

We proposed the use of nonharmonic analysis (NHA) to reduce the influence of the analytical window length and to achieve a tradeoff between the time and frequency resolutions. NHA has already proved effective in image signal processing [33], [34], audio [35], video [36], stock price fluctuation [37], and medical tomography technology [38]–[40] applications. Line noise, such as power supply noise and violin modes, is mixed with GW signals, and its amplitude is higher than that of GW signals [41]. Consequently, when GWs are visualized and detected in the time-frequency domain, some GW components are occluded by the line noise, rendering their observation and analysis very difficult. Note that the line noise is generally removed by using a notch filter, but if the notch filter is implemented in the frequency band in which the line noise exists, the GW signal near the line noise is also removed and the original GW characteristics near the line noise will be lost. As NHA achieves a high frequency resolution and noise rejection capability, it is possible to visualize and analyze the GW signal in a noisy environment, and weak GW signal information can be extracted and represented without employing a notch filter.

However, like the GW150914 signal, the frequency changes slowly over a long time in the low frequency band (~ 35 Hz) and then increases rapidly from the low to high frequency band at about 250 Hz over a few milliseconds [2], [42], [43], as the window lengths of the STFT method and many other analysis methods are only suitable for a restricted frequency range; it is difficult to represent this type of signal using a fixed window length. The NHA method can be successfully used to analyze signal over wide frequency ranges by using a fixed window length, because the window length has less influence on NHA than on the STFT method and others. However, as the frequency of signal varies with time inconstantly, the tradeoff between time and frequency resolution becomes difficult.

Therefore, it is important and essential to propose a new time-frequency analysis method to accurately analyze the frequency change of GW signal.

III. MULTIWINDOW NHA

The sources of GW signal may differ, but the basic features are similar. Fig. 1 shows the basic features of GW signal. Figs. 1(a) and (b) present the amplitude and frequency variation of GW signal in the time domain, respectively. As shown

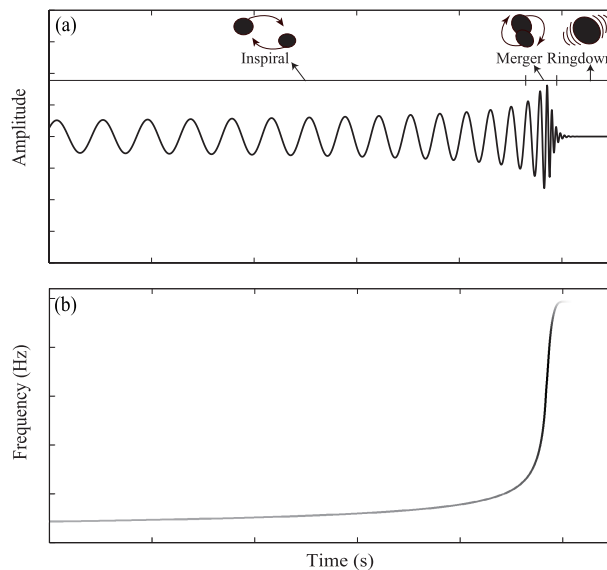


FIGURE 1. Basic features of GW signal. (a) Amplitude variation of GW signal in the time domain, (b) Frequency variation of GW signal in the time domain.

in Fig. 1, the basic features of GW point to it being produced by inspiral and merger, and subsequent final ringdown.

For analyzing the period of inspiral, because the duration is relatively long, the frequency is a low value with little fluctuation, and the signal-to-noise ratio (SNR) is very low, a long analytical window length should be used to improve the frequency resolution and the SNR in low frequency band.

However, as the signal increases rapidly in frequency and amplitude from the low to high frequency band over a short time in the merger period, where the amplitude achieving a maximum enhances the SNR, thus, for accurate analysis and observation of the rapid frequency change of a GW signal, a short analytical window length is essential to improve the time resolution in this period.

Therefore, as the time duration, frequency variation, and the SNR of inspiral and merger are entirely different, it is difficult to assign a consistent window length throughout the entire time duration for GW signal since they are different in different frequency band as shown in Table 1.

Because the amplitude exponentially damps from peak to zero immediately in the period of ringdown even though the frequency is still at its peak, the SNR equals zero immediately [2], [44]–[46]. Thus, it is difficult to observe and visualize the signal in the period of ringdown, and the time-frequency analysis of GW signal points to the periods of inspiral and merger, not ringdown at the present stage.

In order to analyze and observe the GW signal accurately and solve the problem caused by noises and limitations of the above-mentioned methods, we propose a new multiwindow NHA analysis method, in which band division is performed in the frequency domain, the appropriate window length is assigned for each subband, and the standard NHA is performed to analyze and represent a GW signal at the

TABLE 1. Time duration and frequency variation and signal-to-noise ratio and appropriate window length in the periods of inspiral and merger.

	Inspiral	Merger
Time duration	Long	Short
Frequency variation	Slowly	Rapidly
Signal-to-noise ratio	Low	High
Appropriate window length	Long	Short

appropriate window length for each subband by conducting the following steps.

Algorithm 1 Flow Chat of Multiwindow NHA

- 1: Determine the parameters for performing octave band division,
- 2: Perform band division by using the bandpass filter for the determined band,
- 3: Set the appropriate window length for each subband and perform NHA,
- 4: Summarize and plot the analyzed data of each subband.

As a consequence, multiwindow NHA can inherit the specific advantages of NHA, minimize the influence of the analytical window length and the noise, and substantially improve the time and frequency resolutions.

A. NHA METHOD DESCRIPTION

The STFT as a Fourier-related transform has been commonly used for frequency analysis, in which the Fourier transform can be represented as follows:

$$X(nf_1) = \frac{1}{T} \int_0^T x(t) e^{-j2\pi nf_1 t} dt, \quad (1)$$

where T is the analytical window length ($f_1 = 1/T$, n is a positive integer). Equation (1) is solved to determine the Fourier coefficients. As the Fourier transform is used for analyzing a completely periodic signal in an analysis window T , thus, the calculated frequencies (nf_1) depend on the window length T , and errors frequently occur in the analysis of non-harmonic signal frequencies. Moreover, if the length of the analysis window is decreased to increase the time resolution, the frequency resolution also decreases [33].

As the Fourier coefficients are estimated based on the least squares method, NHA enables an accurate estimation of the frequency f , amplitude A , and initial phase φ , avoiding the dominance of the analytical window length. To minimize the sum of squares of the difference between the object signal and the sinusoidal model signal, f , A , and φ are calculated using the cost function, as follows:

$$F(A, f, \varphi) = \frac{1}{N} \sum_{n=0}^{N-1} \{x(n\Delta t) - A \cos(2\pi fn\Delta t + \varphi)\}^2, \quad (2)$$

where N is the total number of samples and Δt is the sampling interval ($\Delta t = 1/f_s$; here, f_s is the sampling frequency).

In this way, NHA can reduce the effect of the analytical window length and can predict surrounding information from a part of the signal. Therefore, we apply the nonlinear equation process to (2) to perform the optimum calculation of the final value of f , as well as the parameters A and φ .

By considering (2) as a cost function, this nonlinear optimization can be formulated as a minimization problem. In this formulation, \hat{f}_m and $\hat{\varphi}_m$ are determined using the steepest descent method, producing the following expressions:

$$\hat{f}_{m+1} = \hat{f}_m - \mu_m \frac{\partial F}{\partial f}, \quad (3)$$

$$\hat{\varphi}_{m+1} = \hat{\varphi}_m - \mu_m \frac{\partial F}{\partial \varphi}. \quad (4)$$

We use the following shorthand to express (3) and (4):

$$\partial F = \partial F(\hat{A}_m, \hat{f}_m, \hat{\varphi}_m). \quad (5)$$

A can be uniquely determined only if \hat{f}_m and $\hat{\varphi}_m$ are known. The following formula is used to cause A to converge:

$$\hat{A}_{m+1} = \hat{A}_m - \mu_m \frac{\partial F}{\partial A}, \quad (6)$$

where μ_m is a weighting coefficient based on the retardation method and has a value between 0 and 1. This parameter is used to convert cost functions, calculated by using recurrence formulas, into a monotonically decreasing sequence [47], [48].

This series of calculations is repeated so that \hat{A}_m , \hat{f}_m , and $\hat{\varphi}_m$ converge with high accuracy. Although the steepest descent method causes values to converge over a comparatively wide range, a single series of operations is unable to ensure sufficient accuracy. To achieve highly accurate conversion, NHA improves the accuracy by applying Newton's method after the application of the steepest descent method. The following recurrence formula is used for Newton's method:

$$\hat{f}_{m+1} = \hat{f}_m - \frac{v_m}{J} \begin{vmatrix} \frac{\partial F}{\partial f} & \frac{\partial^2 F}{\partial f \partial \varphi} \\ \frac{\partial F}{\partial \varphi} & \frac{\partial^2 F}{\partial \varphi^2} \end{vmatrix}, \quad (7)$$

$$\hat{\varphi}_{m+1} = \hat{\varphi}_m - \frac{v_m}{J} \begin{vmatrix} \frac{\partial^2 F}{\partial f^2} & \frac{\partial F}{\partial f} \\ \frac{\partial^2 F}{\partial f \partial \varphi} & \frac{\partial F}{\partial \varphi} \end{vmatrix}, \quad (8)$$

where

$$J = \begin{vmatrix} \frac{\partial^2 F}{\partial f^2} & \frac{\partial^2 F}{\partial f \partial \varphi} \\ \frac{\partial^2 F}{\partial \varphi^2} & \frac{\partial^2 F}{\partial \varphi^2} \end{vmatrix}. \quad (9)$$

Equations (7)–(9) can be written as

$$\partial^2 F = \partial^2 F(\hat{A}_m, \hat{f}_m, \hat{\varphi}_m), \quad (10)$$

where μ_m and v_m are weighting coefficients that are based on the retardation method [49], [50]. After applying (7) and (8), \hat{A}_m is made to converge by applying (6) in the same

manner as the steepest descent method and the series of calculations is repeated. Thus, the frequency parameters are quickly estimated to a high degree of accuracy by employing a hybrid process that combines the steepest descent method with Newton's method.

Even in a case where there are several sinusoidal waves, the spectral parameters can be approximately derived by sequential reduction in which the extraction principle is that the amplitude of frequency component which owns the largest value will be extracted every time, and the same process will be implemented in the rest frequency components until the extraction will be repeated for J times. Here, $x(n)$ is expressed as the sum of J sinusoidal waves in the following manner:

$$x(n) = \sum_{j=1}^J \{A_j \cos(2\pi f_j n \Delta t + \varphi_j)\}, \quad (11)$$

According to Parseval's theorem, the object signal frequency f_j and the model signal's frequency \hat{f} do not match at all; that is, if

$$f_j \neq \hat{f}, \quad (12)$$

then

$$F(\hat{A}, \hat{f}, \hat{\varphi}) = \hat{A}^2 + \sum_{j=1}^J \hat{A}_j^2. \quad (13)$$

In addition, if the pair of \hat{f} and $\hat{\varphi}$ matches either f_j or φ_j , then

$$F(\hat{A}, \hat{f}, \hat{\varphi}) = (\hat{A}^2 - A_j)^2 + \sum_{k=1, k \neq j}^K \hat{A}_k^2, \quad (14)$$

If both A_j and \hat{A} match, a frequency component of an estimated spectrum can be erased completely from an object signal. Therefore, the problem of acquiring an optimum solution is frequency-independent and is applicable to a signal consisting of several sinusoidal waves by sequential and individual estimation from the object signal. In other words, even when the object signal is a composite sinusoidal wave, several sinusoidal waves can be extracted by performing similar processing on sequential residual signals [35].

According to these analyses, the NHA method differs from the integral-method-based Fourier transform technique because its accuracy does not depend on the analytical window length; thus, the frequency and other associated parameters can be calculated accurately and side lobes are not generated.

For example, Figs. 2 and 3 show the spectrum analysis results of a sinusoidal wave model processed using the FFT and NHA techniques. The signal in time $t = 1$ s has amplitude $A = 1$ and frequencies (Fig. 2) $f = 2$ Hz and (Fig. 3) $f = 2.5$ Hz. Three frequency components were estimated in each time interval using NHA since both Figs. 2 and 3 have one frequency merely. Both methods provide accurate estimates when the waveform frequency is an

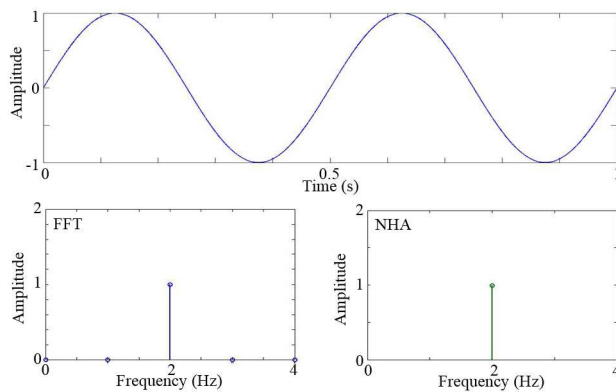


FIGURE 2. Spectrum analysis results for a signal with an integer waveform frequency in time $t = 1$ s obtained using the FFT and NHA methods. Amplitude $A = 1$ and frequency $f = 2$ Hz.

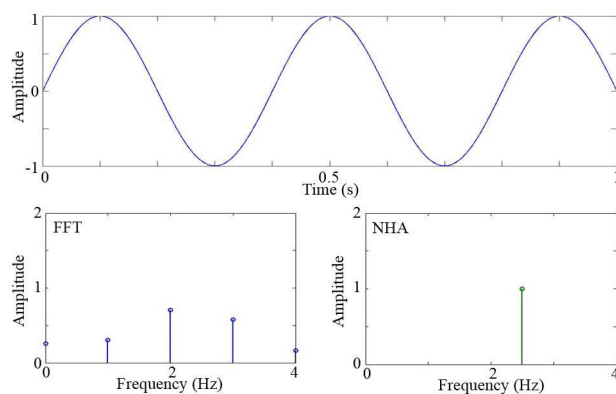


FIGURE 3. Spectrum analysis results for a signal with a noninteger waveform frequency in time $t = 1$ s obtained using the FFT and NHA methods. Amplitude $A = 1$ and frequency $f = 2.5$ Hz.

integer, as shown in Fig. 2. However, as the GW signal frequency changes inconstantly with time and the orthogonality of sinusoidal wave does not hold within incomplete periods, if the frequency of a particular waveform is not an integer, such as the case shown in Fig. 3, owing to the influence of the analysis window, side lobes appear, and the amplitude disperses into components in adjacent frequency bands when the FFT method is used. However, as NHA can overcome the influence of the analytical window length, side lobes will not appear, and even if three frequency components were estimated in each time interval, only one frequency component was showed, the rest two are equal to zero; thus, the values of amplitude and frequency can be estimated accurately.

Therefore, NHA can be employed to track the frequency changes finely and achieve high frequency resolution.

B. OCTAVE DIVISION METHOD

Many GW signals, including the GW150914 signal, show low-frequency characteristics over a long time and rapid low-to-high frequency variations. Therefore, both high frequency resolution and high time resolution are essential. However, as it is difficult to extract GW signal characteristics in detail

by equally dividing the frequency band, we used octave division to subdivide the frequency band finely.

As the highest analytical frequency has been determined in advance, if the frequency band partitioning is performed from the highest frequency to low frequency, the frequency band can be evenly divided proportionally until 0 Hz, but not vice versa. Therefore, the frequency band partitioning is performed according to the necessary number of subbands and the division is performed from high to low frequency. Considering the characteristics of GW signal, for the highest frequency f_0 , the analytical frequency range of the highest-frequency subband is the widest, and the widths of subsequent frequency subbands decrease in proportion to the frequency. Let f_k be the lower band limit of the k -frequency sub-band, which can be calculated for a proportional factor $\frac{n}{m}$ as

$$f_k = \left(\frac{m}{n+m} \right)^k f_0. \quad (15)$$

Moreover, it is necessary to assign an appropriate analytical time interval to each frequency subband. For the lowest-frequency subband, the analytical time interval should be the largest, and the higher the frequency subband, the shorter its analytical time interval. The analytical time interval t_k is the inverse of the lower band limit of the k -frequency sub-band calculated as

$$t_k = \frac{1}{f_k}. \quad (16)$$

As the lower band limit of the last subband is zero, we set the analytical time interval of the last subband to be 1.5 times longer than that of the penultimate interval.

IV. COMPARISON OF NHA AND MULTIWINDOW NHA

Binary star coalescence events are among the primary targets of global GW detectors. GW150914 is a recorded GW signal that is believed to have been produced by the coalescence of two black holes [43]. As the chirp wave that is characteristic of a GW signal generated by binary star coalescence, a simulation signal with a frequency that first changed a little in a low value over a long time and then increased rapidly from low to high over a short time was created by:

$$f = \frac{1}{(1-t)^2}, \quad (17)$$

where t is the duration of signal and f is the frequency. As the frequency of GW150914 signal increased drastically in a short time, the peak of frequency is below 300 Hz, and the sampling frequency is 4096 Hz; the simulation signal duration was $t = 1$ s, the maximum frequency was $f = 300$ Hz, and the sampling frequency was $f_s = 4096$ Hz.

Fig. 4 shows the simulation signal results processed by NHA for different window lengths and multiwindow NHA. Fig. 4(a) depicts the simulation signal in the time domain, and Figs. 4(b), (c), and (d) present the NHA results obtained for window lengths of 32 samples (0.0078 s), 128 samples (0.0313 s), and 512 samples (0.1250 s), respectively. For simplicity, we name them NHA(32), NHA(128), and NHA(512).

Fig. 4(e) presents the analysis results obtained by performing multiwindow NHA. The curve of equation (17) was plotted on each graph as a red line. Whether using NHA for different window lengths or multiwindow NHA, we have estimated ten frequency components in each time interval because the amplitude ratio between the largest and lowest components is 10^{-3} (-60dB).

Fig. 4(b) shows how a short window length can be used to analyze high frequencies of up to 300 Hz accurately. Although fast frequency changes are correctly analyzed in the higher-frequency range, as the frequency change of the signal is rather small over a long time in the lower-frequency range, it is difficult to accurately estimate the periodic change of the signal within each analysis interval using a short window length; spectral artifacts may occur that significantly impact the accuracy of the results in the low-frequency range. In particular, if the amplitude is close to zero as shown on the vertical axis of Fig. 4(a), the estimation of frequency change is the most difficult and it is the intersecting point between positive and negative at this moment that caused the great fluctuation.

Fig. 4(c) exhibits poor results in the high-frequency range compared to those in Fig. 4(b), while the distortions in the low-frequency range are reduced since the window length is longer.

Fig. 4(d) displays better low-frequency results than Figs. 4(b) and 4(c) as the window length is longer. However, the high-frequency range results (up to a maximum frequency of 300 Hz) gradually worsen owing to the decreasing time resolution. Consequently, a trade-off exists between the window length and frequency range.

For a stationary signal which has a frequency that changes slowly, NHA can perform analysis using a long window length; whereas if the frequency changes rapidly, as NHA does not depend on the window length, it can analyze the signal using a short window length; however, STFT cannot due to the effect of window length. However, as the GW signal is not a stationary signal (the frequency change is not constant), using a fixed window length to analyze the frequency change of GW signal over the entire frequency range is not appropriate; thus, the errors will appear in different frequency ranges by using different window lengths, even if the NHA does not depend on the window length.

In the case of multiwindow NHA shown as Fig. 4(e), for detailed analysis, the band division is defined by a maximum frequency $f_0 = 300$ Hz, $\frac{n}{m} = \frac{1}{3}$ octave, and 16 divisions, and each frequency subband and its analytical time interval and window length are shown in Table 2. Compared with NHA over the entire frequency range, multiwindow NHA can assign appropriate window lengths and accurately represent the low-to-high frequency changes of the signal while significantly suppressing distortions over the entire frequency range and the analyzed results are highly coincident with the curve of equation (17). Therefore, multiwindow NHA as an analysis method is effective for GW signal processing.

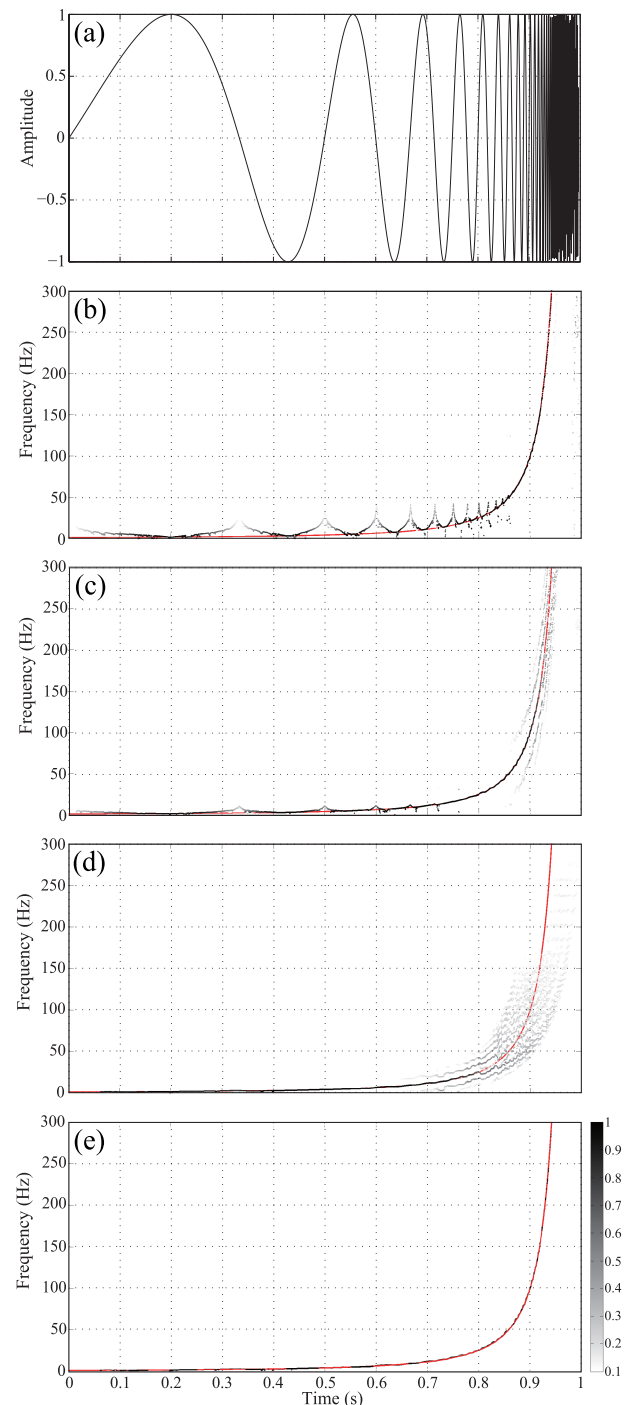


FIGURE 4. Simulation signal analysis results by performing NHA and multiwindow NHA. (a) Time domain waveform, (b) NHA for a window length of 32 samples (0.0078 s), (c) NHA for a window length of 128 samples (0.0313 s), (d) NHA for a window length of 512 samples (0.1250 s), and (e) multiwindow NHA for a band division defined by $f_0 = 300$ Hz, $\frac{n}{m} = \frac{1}{3}$ octave, and 16 divisions. The curve of equation (17) was plotted on graphs(b)-(e) as a red line.

As the frequency reaches 300 Hz at 0.942 s approximately, a frequency component with the maximum amplitude of NHA(32), NHA(128), NHA(512), and multiwindow NHA results was extracted at each time point in the 0.942 s period

TABLE 2. Frequency subbands and Their analytical time intervals and window lengths for simulation signal.

Frequency subband (Hz)	Analytical time interval (s)	Analytical window length (sampling points)
225–300	0.0044	18
169–225	0.0059	24
127–169	0.0079	32
95–127	0.0105	43
71–95	0.0141	58
53–71	0.0189	77
40–53	0.025	102
30–40	0.0333	137
23–30	0.0435	178
17–23	0.0588	241
13–17	0.0769	315
10–13	0.1	410
8–10	0.125	512
6–8	0.1667	683
5–6	0.2	819
0–5	0.3	1229

from 0 s to 0.942 s. In addition, the curve of equation (17) in the same time period was extracted and used as the datum line.

The frequency errors of the NHA(32), NHA(128), NHA(512), and multiwindow NHA results were calculated by:

$$e = \sqrt{\frac{\sum_{m=1}^M [f(m) - \hat{f}(m)]^2}{M}}, \quad (18)$$

where e is the mean frequency error of the extracted interval of the NHA(32), NHA(128), NHA(512), or multiwindow NHA results and the datum line; M is the number of NHA(32), NHA(128), NHA(512), multiwindow NHA, and datum line data in the extracted interval; $f(m)$ is the NHA(32), NHA(128), NHA(512), or multiwindow NHA data in the extracted interval; and $\hat{f}(m)$ is the datum line data in the extracted interval.

In the case of NHA(32), NHA(128), and NHA(512), the mean frequency error of this interval is 10.458 Hz, 13.980 Hz, and 15.097 Hz, respectively. However, the mean frequency error in the multiwindow NHA case is 6.311 Hz. Thus, the analytical precision of multiwindow NHA is quite high, whose error is distinctly less than the NHA(32), NHA(128), and NHA(512) errors.

In conclusion, multiwindow NHA is effective for obtaining accurate spectral representations of signals whose characteristics are similar to the GW.

V. GW150914 SIGNAL ANALYSIS

GW signals include superimposed noise originating from numerous sources, such as ground vibrations [51], [52]. Therefore, the analysis must be applied to and validated for the model signal as well as an actual signal with noise. A GW

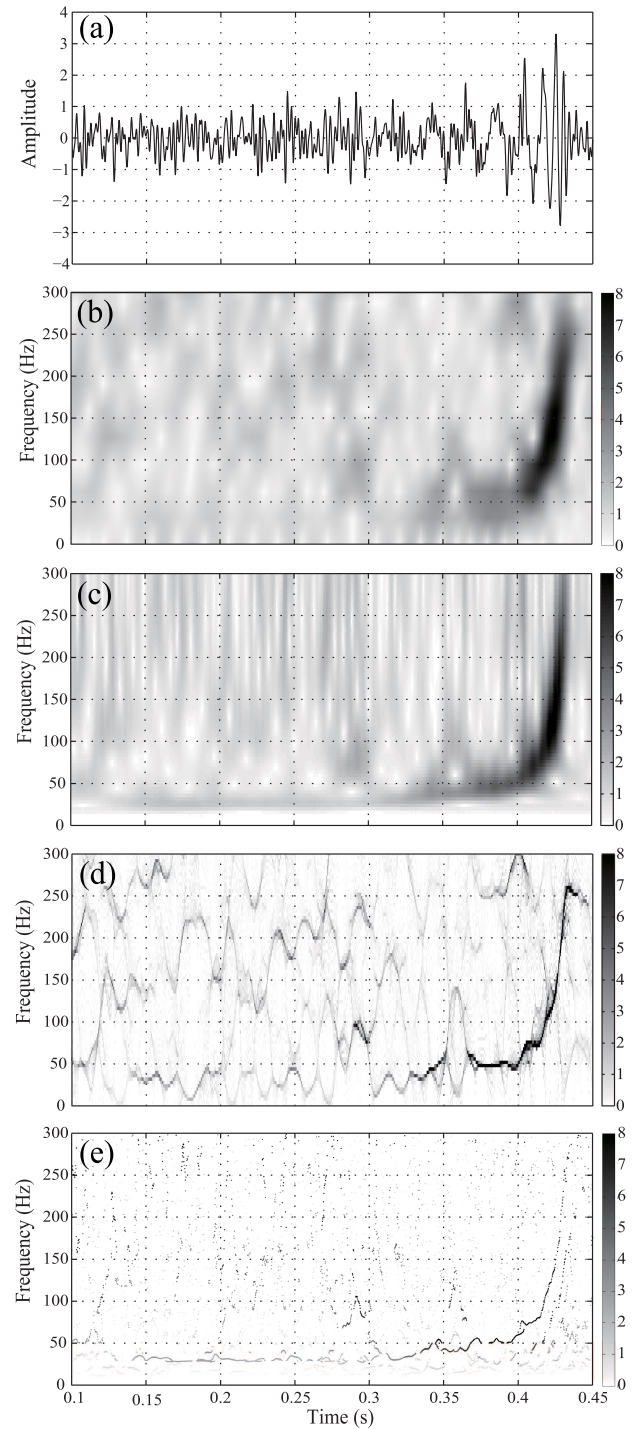


FIGURE 5. Time-frequency analysis results of GW150914. (a) Time domain waveform, (b) STFT results obtained using a window length of 128 samples (0.0313 s), (c) wavelet transform results obtained using a window length of 512 samples (0.1250 s), (d) FSST4 results obtained using a window length of 1024 samples (0.25 s), and (e) multiwindow NHA results obtained for a band division defined by $f_0 = 500$ Hz, $\frac{n}{m} = \frac{1}{3}$ octave, and 19 divisions.

detector has an amplitude detection limit that is defined by a sensitivity curve specific to each frequency range [2].

The duration of GW150914 data (H-H1 LOSC-4 V1-1126259446-32.txt) [53] is 32 s, and it was cut into

a 0.7-s period from 16 s to 16.7 s, where the GW signal frequency peaks at 16.44 s [54]. To limit the influence of noise, we performed whitening in the frequency domain in a manner similar to the analysis procedure applied to the GW150914 signal [55]. The noise-containing GW signal was divided by the LIGO sensitivity curve, and the data were analyzed using the STFT, wavelet transform, FSST4, and multiwindow NHA methods.

Fig. 5 shows the analysis results obtained for GW150914 using the above-mentioned methods, with the sampling frequency $f_s = 4096$ Hz and a processed signal duration $t = 0.7$ s. Although the analytical window length for each method was different, the results shown for each method are the best obtained for the given analytical window length. For simplicity, we only present the analysis results from 0.1 s to 0.45 s and 0 Hz to 300 Hz.

Fig. 5(a) depicts the signal after time-domain whitening, which is still clearly noisy.

Fig. 5(b) shows the analysis results obtained using the STFT method with Hann window. After the black hole merger, a rapid frequency change occurs at 0.4 s [2]. However, the GW signal in the low-frequency range (0–50 Hz) before coalescence cannot be represented using this method because its frequency resolution is poor and the SNR is low, and thus it is difficult to separate the GW signal and noises during this period.

Fig. 5(c) presents the analysis results obtained using the wavelet transform method. As in the STFT technique, the rapid frequency changes in the frequency range of 50–300 Hz were represented in the wavelet transform method. However, the GW signal appears with a wide shadow, so the frequency changes cannot be observed or analyzed in detail. Moreover, the part where the GW signal does not exist appears as a spike, demonstrating that the influence of noise is strong.

Fig. 5(d) shows the analysis results obtained using the new **FSST4 method**, which is the best FSST reconstruction method. In [28], the window length was set to an optimum of 1024 samples (0.25 s); therefore, this window length was also used in this study. Although the GW signal appears as a continuous line in the FSST4 results, the noise also appears as continuous line segments. Moreover, the FSST4 performance is sensitive to the preprocessing method, but preprocessing such as band-rejection filtering was not performed in this study; thus, starting from 0.3 s, the GW signal is not represented continuously in the FSST4 results, as the signal exhibits fluctuations due to noise at approximately 0.36 s. Therefore, the noise immunity of the FSST4 method is insufficient, and the GW signal could not be visualized in the low-frequency range.

Fig. 5(e) depicts the analysis results obtained by performing multiwindow NHA. For detailed analysis and to reduce the impact of noise, the band division was defined by a maximum frequency $f_0 = 500$ Hz, $\frac{n}{m} = \frac{1}{3}$ octave, and 19 divisions. Similarly, ten frequency components were estimated in each time interval at this time, and each frequency subband and

TABLE 3. Frequency subbands and their analytical time intervals and window lengths for the GW150914 signal.

Frequency subband (Hz)	Analytical time interval (s)	Analytical window length (sampling points)
375–500	0.0027	11
281–375	0.0036	15
211–281	0.0047	19
158–211	0.0063	26
119–158	0.0084	34
89–119	0.0112	46
67–89	0.0149	61
50–67	0.02	82
38–50	0.0263	108
29–38	0.0345	141
22–29	0.0455	186
17–22	0.0588	241
13–17	0.0769	315
10–13	0.1	410
8–10	0.125	512
6–8	0.1667	683
5–6	0.2	819
4–5	0.25	1024
0–4	0.375	1536

its analytical time interval and window length are shown in Table 3. Compared to the other three techniques, multiwindow NHA shows significant superiority as it is the only technique that enabled accurate and clear representation of the signal from low to high frequency without noise-induced fluctuations from approximately 0.14 s before black hole coalescence. Moreover, by using the high time and frequency resolutions, the GW signal could be visualized as a continuous line with an extremely narrow shadow and the noise appears as a point. Thus, the time-frequency information is easily observable and could be analyzed in detail. In addition, as the appropriate window length was assigned by multiwindow NHA for each frequency subband, the GW signal could be separated accurately from high-level noise, indicating that multiwindow NHA enables high noise rejection.

VI. DISCUSSION

The ratio of the GW amplitude in the low-frequency range (0–50 Hz) to that in the high-frequency range in multiwindow NHA is about 0.083, which confirms that the wavelet transform can reproduce the signal in the low-frequency range since the amplitude ratio is basically consistent. However, as the visualization is very blurred, it is difficult to observe the frequency change of the GW in the low-frequency range using wavelet transform.

The FSST technique is a newly proposed analytical method that has some advantages, as evidenced by the numerical processing of synthetic and observed GW signals [28]. Moreover, the GW signal was visualized with a narrow shadow; thus, the FSST4 analysis results were selected for comparison.

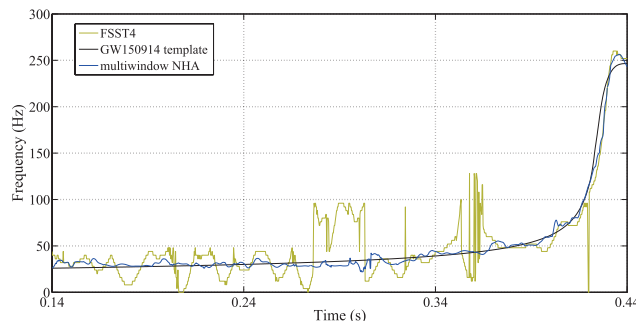


FIGURE 6. Spectra estimated using the FSST4 method, multiwindow NHA, and GW150914 template [56] for 0.3 s before the frequency peak. The mean frequency errors of the FSST4 and multiwindow NHA results are 21.816 Hz and 6.021 Hz, respectively.

As the GW signal could be correctly represented from approximately 0.14 s duration by multiwindow NHA and the GW signal frequency peaked at 0.44 s in the truncation data of GW150914, a frequency component with the maximum amplitude of FSST4 and multiwindow NHA results was extracted at each time point in the 0.3 s period from 0.14 s to 0.44 s.

The template data (GW150914_4_template.hdf5) [56] describe the theoretical waveform summarized by LIGO and Virgo based on the characteristics of GW150914 with the sampling frequency $f_s = 4096$ Hz. As the template extends to 16 s and the frequency peaked at 16 s [54], the template data in the 0.3 s period from 15.7 s to 16 s were extracted and used as the datum line.

Fig. 6 shows the FSST4, multiwindow NHA, and GW150914 template extraction results for 0.3 s before the frequency peak. For simplicity, the datum line is shown for the FSST4 and multiwindow NHA extraction results and a single time axis is used for the FSST4 and multiwindow NHA results. Note that there are two time points of FSST4 without the data of analyzed result at about 0.42 s, consequently, located at 0 Hz causes the huge notch which cannot be seen distinctly in Fig. 5.

The frequency errors of both the FSST4 and multiwindow NHA results were calculated using equation (18), in which e is the mean frequency error of the extracted interval between the FSST4 or multiwindow NHA results and the datum line; M is the number of FSST4, multiwindow NHA, and datum line data in the extracted interval; $f(m)$ is the FSST4 or multiwindow NHA data in the extracted interval; and $\hat{f}(m)$ is the datum line data in the extracted interval.

In the case of FSST4, the mean frequency error of this interval is 21.816 Hz. However, the mean frequency error in the multiwindow NHA case is 6.021 Hz. Thus, the multiwindow NHA error is less than a third of the FSST4 error, which is the most advanced proposed method thus far, and the analytical precision of multiwindow NHA is quite high even with significant noise.

Therefore, multiwindow NHA affords high time-frequency resolution, analytical precision, and noise reduction.

VII. CONCLUSION

Generalization of the GW150914 signal observations indicates that many GW signals may exhibit low-frequency characteristics over a long time and rapid low-to-high frequency variations, making signal representation difficult in the frequency domain owing to the trade-off relationship between time and frequency resolution specific to standard frequency analysis methods. Moreover, appropriate window length assignment is essential to enable accurate processing of a signal with long slow changing and rapidly changing frequency. Signals cannot be represented accurately in both the low- and high-frequency ranges by performing analysis using a fixed window length, whereas multiwindow NHA can be employed to analyze and represent GW signals accurately by using band division and assigning close-to-optimum window lengths from the low- to high-frequency range.

The GW150914 signal analysis results exhibited strong noise throughout the frequency band regardless of the methods used. However, the GW signal could not be correctly and clearly represented in the low-frequency range using the STFT, wavelet transform, and FSST4 methods; only by using multiwindow NHA could the GW signal be correctly and clearly represented without noise fluctuations in the low-frequency range. The multiwindow NHA results also exhibited improved representation and reproducibility for fast frequency changes over time in the mid- and high-frequency ranges. In addition, near the time of black hole coalescence when the GW frequency changes rapidly, the window can be made narrower, the time resolution can be improved, and the influence of noise can be suppressed by employing multiwindow NHA.

Moreover, the mean frequency error of the multiwindow NHA results was significantly lower than that of the FSST4 results in the 0.3 s period before coalescence when the frequency peaked. Thus, even with the presence of significant noise, the analytical precision of multiwindow NHA remains high.

Consequently, multiwindow NHA can be utilized to represent GW signals from the low- to high-frequency range accurately based on the high time-frequency resolution and analytical precision, and the influence of noise can be suppressed more effectively than if state-of-the-art methods were used.

In the future, we will employ multiwindow NHA to analyze data from LIGO, KAGRA, and other GW observation systems.

VIII. ACKNOWLEDGMENT

The authors would like to thank Masaya Nakano and Kyohei Miyake for their contribution at the early phase of this work.

REFERENCES

- [1] A. Einstein, “Approximative integration of the field equations of gravitation,” *Sitzungsber. Preuss. Akad. Wiss. Berlin.*, vol. 1916, pp. 688–696, Jul. 1916.
- [2] B. P. Abbott *et al.*, “Observation of gravitational waves from a binary black hole merger,” *Phys. Rev. Lett.*, vol. 116, no. 6, 2016, Art. no. 061102.

- [3] B. P. Abbott *et al.*, "Astrophysical implications of the binary black hole merger GW150914," *Astrophys. J. Lett.*, vol. 818, no. 2, 2016, Art. no. L22.
- [4] B. P. Abbott *et al.*, "Properties of the binary black hole merger GW150914," *Phys. Rev. Lett.*, vol. 116, no. 24, 2016, Art. no. 241102.
- [5] B. P. Abbott *et al.*, "LIGO: The laser interferometer gravitational-wave observatory," *Rep. Prog. Phys.*, vol. 72, no. 7, 2009, Art. no. 076901.
- [6] A. Abramovici *et al.*, "LIGO: The laser interferometer gravitational-wave observatory," *Science*, vol. 256, no. 5055, pp. 325–333, 1992.
- [7] F. Acernese *et al.*, "Search for inspiralling binary events in the Virgo engineering run data," *Classical Quantum Gravity*, vol. 21, no. 5, 2004, Art. no. S709.
- [8] F. Acernese *et al.*, "The Virgo status," *Classical Quantum Gravity*, vol. 23, no. 19, 2006, Art. no. S635.
- [9] K. Somiya, "Detector configuration of KAGRA—the Japanese cryogenic gravitational-wave detector," *Classical Quantum Gravity*, vol. 29, no. 12, 2012, Art. no. 124007.
- [10] Y. Aso *et al.*, "Interferometer design of the KAGRA gravitational wave detector," *Phys. Rev. D, Part. Fields*, vol. 88, no. 4, 2013, Art. no. 043007.
- [11] B. Abbott *et al.*, "Search for gravitational waves from binary inspirals in S3 and S4 LIGO data," *Phys. Rev. D, Part. Fields*, vol. 77, no. 6, 2008, Art. no. 062002.
- [12] *LIGO Scientific Collaboration*. Accessed: Jun. 12, 2018. [Online]. Available: <https://www.ligo.org/science/GW-Inspiral.php>
- [13] B. P. Abbott *et al.*, "GW151226: Observation of gravitational waves from a 22-solar-mass binary black hole coalescence," *Phys. Rev. Lett.*, vol. 116, no. 24, 2016, Art. no. 241103.
- [14] B. P. Abbott *et al.*, "GW170104: Observation of a 50-solar-mass binary black hole coalescence at redshift 0.2," *Phys. Rev. Lett.*, vol. 118, no. 22, 2017, Art. no. 221101.
- [15] B. P. Abbott *et al.*, "GW170608: Observation of a 19 solar-mass binary black hole coalescence," *Astrophys. J. Lett.*, vol. 851, no. 2, 2017, Art. no. L35.
- [16] B. P. Abbott *et al.*, "GW170814: A three-detector observation of gravitational waves from a binary black hole coalescence," *Phys. Rev. Lett.*, vol. 119, no. 14, 2017, Art. no. 141101.
- [17] B. P. Abbott *et al.*, "GW170817: Observation of gravitational waves from a binary neutron star inspiral," *Phys. Rev. Lett.*, vol. 119, no. 16, 2017, Art. no. 161101.
- [18] É. É. Flanagan and S. A. Hughes, "Measuring gravitational waves from binary black hole coalescences. II. The waves' information and its extraction, with and without templates," *Phys. Rev. D, Part. Fields*, vol. 57, no. 8, pp. 4566–4587, 1998.
- [19] B. J. Owen and B. S. Sathyaprakash, "Matched filtering of gravitational waves from inspiraling compact binaries: Computational cost and template placement," *Phys. Rev. D, Part. Fields*, vol. 60, no. 2, 1999, Art. no. 022002.
- [20] J. N. Yang, Y. Lei, S. Lin, and N. Huang, "Hilbert-Huang based approach for structural damage detection," *J. Eng. Mech.*, vol. 130, no. 1, pp. 85–95, 2004.
- [21] N. A. Lockerbie and K. V. Tokmakov, "A 'Violin-Mode' shadow sensor for interferometric gravitational wave detectors," *Meas. Sci. Technol.*, vol. 25, no. 12, 2014, Art. no. 125110.
- [22] B. P. Abbott *et al.*, "GW150914: Implications for the stochastic gravitational-wave background from binary black holes," *Phys. Rev. Lett.*, vol. 116, no. 13, 2016, Art. no. 131102.
- [23] L. S. Finn, "Aperture synthesis for gravitational-wave data analysis: Deterministic sources," *Phys. Rev. D, Part. Fields*, vol. 63, no. 10, 2001, Art. no. 102001.
- [24] *LIGO Document T020043-x0*. Accessed: Jun. 12, 2018. [Online]. Available: <https://dcc.ligo.org/T020043/public>
- [25] J. Sylvestre, "Time-frequency detection algorithm for gravitational wave bursts," *Phys. Rev. D, Part. Fields*, vol. 66, no. 10, 2002, Art. no. 102004.
- [26] F. Zink and R. A. Vincent, "Wavelet analysis of stratosphere gravity wave packets over Macquarie Island. I. Wave parameters," *J. Geophys. Res.*, vol. 106, no. D10, pp. 10275–10288, 2001.
- [27] S. Klimenko and G. Mitselmakher, "A wavelet method for detection of gravitational wave bursts," *Classical Quantum Gravity*, vol. 21, no. 20, pp. S1819–S1830, 2004.
- [28] D.-H. Pham and S. Meignen, "High-order synchrosqueezing transform for multicomponent signals analysis—with an application to gravitational-wave signal," *IEEE Trans. Signal Process.*, vol. 65, no. 12, pp. 3168–3178, Jun. 2017.
- [29] D. J. A. McKechnie, C. Robinson, and B. S. Sathyaprakash, "A tapering window for time-domain templates and simulated signals in the detection of gravitational waves from coalescing compact binaries," *Classical Quantum Gravity*, vol. 27, no. 8, 2010, Art. no. 084020.
- [30] Z. Can, Z. Aslan, O. Oguz, and A. H. Siddiqi, "Wavelet transforms of meteorological parameters and gravity waves," *Ann. Geophys.*, vol. 23, no. 3, pp. 659–663, 2005.
- [31] L. Lei, C. Wang, and X. Liu, "Discrete wavelet transform decomposition level determination exploiting sparseness measurement," *Int. J. Electr. Comput., Energetic, Electron. Commun. Eng.*, vol. 7, no. 9, pp. 1182–1185, 2013.
- [32] A. S. Chavan and K. Mahesh, "EEG signal preprocessing using wavelet transform," *Int. J. Elec. Eng.*, vol. 3, no. 1, pp. 5–10, 2011.
- [33] M. Hasegawa, T. Kako, S. H. Hirobayashi, T. Misawa, T. Yoshizawa, and Y. Inazumi, "Image inpainting on the basis of spectral structure from 2-D nonharmonic analysis," *IEEE Trans. Image Process.*, vol. 22, no. 8, pp. 3008–3017, Aug. 2013.
- [34] F. Hosotani, Y. Inuzuka, M. Hasegawa, S. Hirobayashi, and T. Misawa, "Image denoising with edge-preserving and segmentation based on mask NHA," *IEEE Trans. Image Process.*, vol. 24, no. 12, pp. 6025–6033, Dec. 2015.
- [35] T. Yoshizawa, S. Hirobayashi, and T. Misawa, "Noise reduction for periodic signals using high-resolution frequency analysis," *EURASIP J. Audio Speech Music Process.*, vol. 2011, no. 1, 2011, Art. no. 5.
- [36] T. Ueda, K. Fujii, S. Hirobayashi, T. Yoshizawa, and T. Misawa, "Motion analysis using 3D high-resolution frequency analysis," *IEEE Trans. Image Process.*, vol. 22, no. 8, pp. 2946–2959, Aug. 2013.
- [37] T. Ichinose, S. Hirobayashi, T. Misawa, and T. Yoshizawa, "Forecast of stock market based on nonharmonic analysis used on NASDAQ since 1985," *Appl. Financial Econ.*, vol. 22, no. 3, pp. 197–208, 2012.
- [38] T. Uchida *et al.*, "Non-uniform non-harmonic analysis method development and verification of applicability to swept source optical coherence tomography," *Nonlinear Theory Appl.*, vol. 4, no. 2, pp. 172–182, 2013.
- [39] X. Cao *et al.*, "Non-harmonic analysis applied to optical coherence tomography imaging," *Jpn. J. Appl. Phys.*, vol. 51, no. 2R, 2012, Art. no. 022503.
- [40] T. Uchida, Y. Inuzuka, M. Hasegawa, S. Hirobayashi, and T. Misawa, "Numerical simulation validation of nonuniform, nonharmonic analysis of spectral-domain optical coherence tomography," *Opt. Eng.*, vol. 54, no. 3, 2015, Art. no. 033108.
- [41] L. S. Finn and S. Mukherjee, "Data conditioning for gravitational wave detectors: A Kalman filter for regressing suspension violin modes," *Phys. Rev. D, Part. Fields*, vol. 63, 2001, Art. no. 062004.
- [42] *LIGO Detects First Ever Gravitational Waves from two Merging Black Holes*: Physicsworld.com. Accessed: Feb. 12, 2016. [Online]. Available: <http://physicsworld.com/cws/article/news/2016/feb/11/ligo-detects-first-ever-gravitational-waves-from-two-merging-black-holes>
- [43] B. P. Abbott *et al.*, "Tests of general relativity with GW150914," *Phys. Rev. Lett.*, vol. 116, May 2016, Art. no. 221101.
- [44] A. Ghosh, W. D. Pozzo, and P. Ajith, "Estimating parameters of binary black holes from gravitational-wave observations of their inspiral, merger and ringdown," *Phys. Rev. D, Part. Fields*, vol. 94, no. 10, 2016, Art. no. 104070.
- [45] A. Maselli, K. D. Kokkotas, and P. Laguna, "Observing binary black hole ringdowns by advanced gravitational wave detectors," *Phys. Rev. D, Part. Fields*, vol. 95, no. 10, 2017, Art. no. 104026.
- [46] E. Thrane, P. D. Lasky, and Y. Levin, "Challenges for testing the no-hair theorem with current and planned gravitational-wave detectors," *Phys. Rev. D, Part. Fields*, vol. 96, no. 10, 2017, Art. no. 102004.
- [47] A. E. Beaton and J. W. Tukey, "The fitting of power series, meaning polynomials, illustrated on band-spectroscopic-data," *Technometrics*, vol. 16, no. 2, pp. 147–185, 1974.
- [48] P. E. Gill and W. Murray, "Quasi-Newton methods for unconstrained optimization," *IMA J. Appl. Math.*, vol. 9, no. 1, pp. 91–108, Feb. 1972.
- [49] E. B. George and M. J. T. Smith, "Speech analysis/synthesis and modification using an analysis-by-synthesis/overlap-add sinusoidal model," *IEEE Trans. Speech Audio Process.*, vol. 5, no. 5, pp. 389–406, Sep. 1997.
- [50] E. B. George and M. J. T. Smith, "Analysis-by-synthesis/overlap add sinusoidal modeling applied to the analysis and synthesis of musical tones," *J. Audio Eng. Soc.*, vol. 40, no. 6, pp. 497–516, 1992.
- [51] S. A. Hughes, "Listening to the universe with gravitational-wave astronomy," *Ann. Phys.*, vol. 303, no. 1, pp. 142–178, 2003.
- [52] B. P. Abbott *et al.*, "Characterization of transient noise in advanced LIGO relevant to gravitational wave signal GW150914," *Classical Quantum Gravity*, vol. 33, no. 13, 2016, Art. no. 134001.

- [53] *Data Release for Event GW150914*. Accessed: Oct. 12, 2017. [Online]. Available: <https://losc.ligo.org/events/GW150914/>
- [54] *LIGO Open Science Center*. Accessed: Feb. 14, 2018. [Online]. Available: https://losc.ligo.org/s/events/GW150914/LOSC_Event_tutorial_GW150914.html
- [55] *LIGO Open Science Center*. Accessed: Oct. 12, 2017. [Online]. Available: https://losc.ligo.org/s/events/GW150914/GW150914_tutorial.html
- [56] *LIGO Open Science Center*. Accessed: Feb. 14, 2018. [Online]. Available: <https://losc.ligo.org/tutorials/>



MASAYA HASEGAWA received the B.E., M.E., and Ph.D. degrees from the University of Toyama in 2012, 2014, and 2017, respectively, and the D.Eng. degree from the University of Toyama. He is currently a Research Assistant Professor at the University of Toyama. His research interests include multidimensional signal analysis, high accuracy analysis, image processing, and medical image analysis.



SHIGEKI HIROBAYASHI received the D.Eng. degree from the University of Toyama. He is currently a Professor at the University of Toyama. He has been engaged in research on acoustic signal processing, acoustic field control, and image processing. He is a member of the Institute of Electronics Information and Communication Engineers, the Institute of Electrical Engineers of Japan, the Acoustic Society of Japan, the Acoustic Society of America, and the IEEE.



HIDEYUKI TAGOSHI is currently an Associate Professor at the Institute for Cosmic Ray Research, The University of Tokyo. His research interests are in gravitational wave physics and astrophysics.



TATSUYA NARIKAWA is currently a Post-Doctoral Fellow at the Department of Physics, Kyoto University. His research interests are in gravitational-wave astrophysics.



NAMI UCHIKATA is currently a Post-Doctoral Researcher at Niigata University. Her research interests include astrophysical theory.



HIROTAKA TAKAHASHI received the D.Sc. degree from the Graduate School of Science and Technology, Niigata University, Japan, in 2005. He was a PD at the Max Planck Institute for Gravitational Physics (Albert Einstein Institute), Germany, from 2005 to 2007. He is currently an Associate Professor with the Department of Information and Management Systems Engineering, Nagaoka University of Technology, Japan. His research interests include the adaptive data analysis methods, information theory, machine learning and gravitational wave physics, and astronomy (general relativity). He is a member of the Institute of Electronics, Information and Communication Engineers and the Physical Society of Japan.



DONGBAO JIA received the M.E. and Ph.D. degrees from the Department of Intellectual Information Engineering, Graduate School of Science and Engineering for Education, University of Toyama, Toyama, Japan, in 2015 and 2018, respectively. He is currently a Lecturer at the School of Computer Engineering, Huaihai Institute of Technology, Lianyungang, China. He is also a special Researcher at the University of Toyama. His main research interests are signal processing, time-frequency analysis, and neural engineering.



KENTA YANAGISAWA received the B.E. degree in intellectual information engineering from the University of Toyama, Toyama, Japan, in 2016, where he is currently pursuing the degree with the Department of Intellectual Information Engineering, Graduate School of Science and Engineering. His research interests include gravitational wave visualization and digital signal processing.



YUTA ONO is currently pursuing the degree with the Department of Intellectual Information Engineering, University of Toyama. His research interests include time-frequency analysis and image processing.



KANNA HIROBAYASHI is currently pursuing the degree with the Department of Intellectual Information Engineering, University of Toyama. Her research interests include signal processing and NMR-imaging.